

MIPS Radiometric Model Correlation After Campaigns D1 - F
MER-IOC-001A

G. H. Rieke and the MIPS Team

October 8, 2003

1. Summary: The first four campaigns for the MIPS 24 μm array provided an opportunity to correlate the MIPS radiometric model based on measurements on the sky. Based on this model, the parameters released to observers to plan use of this band can be revised. Sensitivities *per DCE* and as a function of background and integration time are listed in the table below.

Predicted Sensitivity, one sigma per DCE, in mJy			
	16.1 MJy/sr	23.9 MJy/sr	65.6 MJy/sr
3 sec	473	538	801
4 sec	358	413	632
10 sec	183	218	357
30 sec	105	130	> 50% saturation level

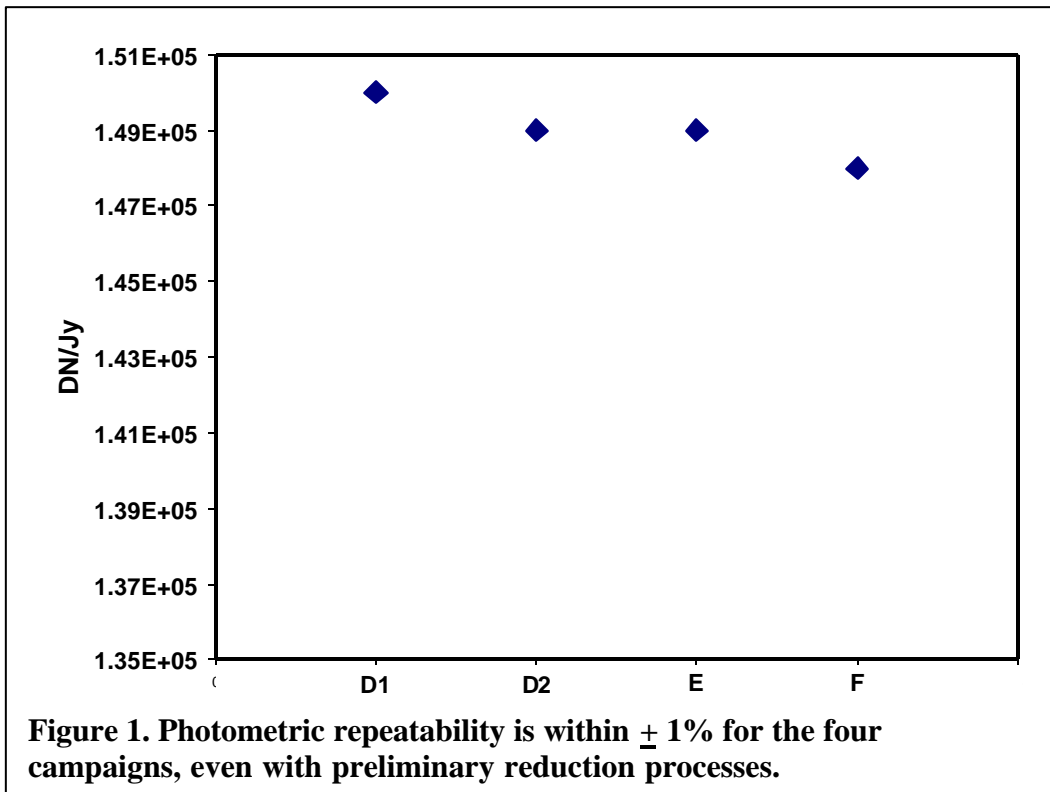
The saturation limit for point sources is 7.8 Jy.

2. Discussion

Campaigns D1 - F provided the first opportunity to compare the on-orbit performance of MIPS with the pre-launch predictions, and to correlate the radiometric model to improve its predictive power.

2.1 Photometric Performance

Even without completion of the calibration of the 24 μm channel, it is performing accurate photometry as shown in Figure 1.



In Campaign E, a variety of stars of different brightnesses and spectral types was observed to search for any systematic trends in the photometric results. Figure 2 shows the data. There are no clear trends. One must also remember that the scatter in this figure may have contributions due to errors in the input flux densities from some of these stars.

There is a hint (perhaps 1.5 standard deviations) of a trend of larger integration slopes being measured with longer integrations. This trend needs to be studied further to see if the calibration can be improved. Nonetheless, the average instrumental throughput measured for these stars, 1.507×10^5 DN.Jy, agrees well with that in Figure 1 from measurements made in the four campaigns, 1.49×10^5 DN/Jy.

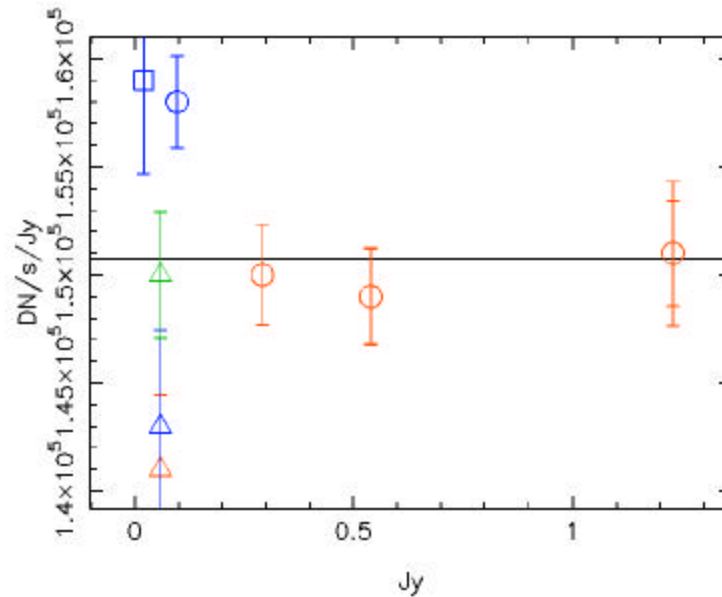


Figure 2. Stellar calibrations plotted vs. the predicted flux density for each star. The weighted mean calibration is plotted as a horizontal line. Cool giants are plotted as circles, A stars as triangles, and solar analogs as squares. 3s integrations are in red, 10s in blue, and 30s in green.

2.2 Response to Extended Emission

For Campaign F, the telescope was sufficiently cold (in fact, below 4K) that the diffuse flux should have been purely from the sky. We have taken the position of HD 159330 to calibrate the response to this flux. Here, the SPOT value for sky flux is 15.3 MJy/sr.

The correlated MIPS radiometric model discussed in Section 2.3 predicts flux densities below the observed values for this field, and this behavior is also seen for other fields. Good agreement requires that the predicted fluxes from the sky be increased by 15%. The nominal errors in this value are about three percentage points. In addition the effect depends on the accuracy of the droop correction. An error of one percentage point in the droop correction would result in about one percentage point error in the sky flux. Thus, the discrepancy appears to lie well outside the identified causes of error. We do not know the source of this additional flux, but in the following we will assume that the effect is real and that predicted sky fluxes should be increased by 15% in computing signal to noise.

2.3 Response to Emission by Telescope

We have compared with signals in the sequence of campaigns with the temperatures measured for the telescope, using the MIPS radiometric model to convert temperatures to signals. A good fit was achieved, assuming that the detector gain is 1 (as opposed to the 0.85 estimated prior to launch), the quantum efficiency is 62.9% (preflight measurement 60%) and the instrument throughput 70% (preflight estimate 66%). The telescope was

taken to be at the temperature of the secondary mirror, and the emissivity was adjusted to optimize the fit, arriving at a final value of 0.184.

We felt that the effective emissivity for the telescope in this band was likely to be close to 0.23. This value arises because the cold Lyot stop in the instrument is 10% oversized, and the areas seen beyond the edge of the telescope exit pupil should all be high emissivity. It is plausible that the somewhat lower emissivity in the fit arises because some of the signal from the telescope arises from surfaces that are colder than the secondary mirror. Specifically, the primary mirror was 2K colder than the secondary, and it and surrounding regions will be "viewed" by the instrument reflected off the secondary. Therefore, in the new model, we fixed the emissivity of the telescope at 0.23 and divided it between the secondary temperature and the primary temperature (2K colder).

A good fit was found with a net emissivity of 10% at the lower temperature and 13% at the higher one. Although there is no direct measurement to constrain these values, they are plausible - implying that the secondary mirror as viewed by MIPS is a few per cent oversized, with other colder emitting areas including the secondary supports and the central baffle on the primary. The view past the edge of the secondary is taken to be black and at the temperature of the secondary. The results of the modeling are listed in Table 1. In addition, we have used the attenuation factor of 300 observed in the 24 micron dark position in Campaign D1 to estimate the background in Campaign C. In this latter campaign, we were unsaturated in the dark position at about 1000 DN/s. Applying a conversion of 5e/DN, we estimate we would have seen 1,500,000 e/s viewing through the telescope (where the data were hard saturated, given the well depth of 320,000 e).

Table 1. Two-Temperature Model vs. Signal		
Campaign	Predicted	Observed
C	2,000,000	~ 1,500,000
D1	8850	8800
D2	2720	2800
E	2300	2400
F	1723	1726

3. Model Assumptions

With a telescope model correlated and performing well on three independent sources of flux, we can look at the instrument sensitivity with greater accuracy than before. In addition, we can assess the uncertainties in these predictions as they are influenced by uncertainties in the model inputs, but with the new constraints.

Table 2. Radiometric Models					
Parameter	Prelaunch	Model 1	Model 2	Model 3	Model 4
Emissivity	0.3	0.23	0.23	0.23	0.23
Telescope Throughput	0.88	0.96	0.96	0.96	0.96
Quantum Efficiency	0.6	0.629	0.629	0.738	0.585
Optical Efficiency	0.66	0.7	0.7	0.7	0.6
DN conversion	5 e/DN	5 e/DN	5 e/DN	5 e/DN	4 e/DN
Photoconductive Gain	0.85	1	1	0.85	1
Read Noise	40e	45e	55e	45e	55e
Sky/minimum sky	1.2	1.38	1.38	1.38	1.38
Sensitivity*	11.0 μ Jy	11.0 μ Jy	11.3 μ Jy	9.6 μ Jy	12.8 μ Jy
* one standard deviation in 2000 seconds of observation					

In the case of emissivity and throughput, the model adjustments remove a slight shade of pessimism injected intentionally in the prelaunch numbers and substitute the values that would be expected for an ideal system. Errors of 5 percentage points in the instrument throughput and of 10 percentage points in the focal plane quantum efficiency would also be within expectations. We have used a calibration of 1.5×10^5 DN/Jy, which appears to be determined to within $\pm 1\%$; this error is small enough that it has not been propagated.

Important assumptions in all the radiometric models used for the values in Table 2 include:

- Minimum zodiacal emission defined by $3.5 \times 10^{-14} B(5500) + 2.9 \times 10^{-8} B(278.5) + 1.78 \times 10^{-5} B(24.45)$. This yields 13 MJy/sr at the MIPS 24 μ m band.
- All predictions from this zodiacal model increased by 15% to allow for extra signal observed on the sky.
- Source extraction by aperture photometry with an aperture diameter of $2.5 \lambda/D$. Encircled energy within this diameter is 67.5% of the [energy incident on the telescope minus the energy absorbed by the central obscuration (which is accounted separately)]. A 10% penalty in sensitivity has been added to allow for the finite pixel size.
- Flat fielding residual noise of 1 part in 10^4 , combined rms with other noise components.
- Cosmic ray hit rate of 0.004/second per pixel
- DCE time of 10 seconds
- Half second dead time for every DCE (one ignore frame)

A further description of the overall model can be found in the MIPS System Description Document.

4. Predicted Sensitivities

4.1 Prelaunch Model

The prelaunch model in Table 2 uses the same source extraction formalism as for the postlaunch models, even though a slightly different formalism was used at the time of the preship review. The difference in the two approaches is less than 1%, and therefore not worth tracking separately. In addition, the sensitivity predicted by the model was degraded by a factor of 1.5 in the numbers propagated by the SSC, to be sure that community science planning would not be upset by on-orbit shortfalls. We show here the predictions with no such adjustment.

4.2 Model 1

Model 1 is the new baseline model. It is adjusted to account for the larger-than-expected throughput of the instrument observed on orbit. There are a variety of ways such adjustments can be made. In this model, we first adjusted the telescope parameters to remove the conservatism in the prelaunch assumptions. We then increased the photoconductive gain to 1 (which is the largest likely value). Since the increased gain does not improve the net instrument quantum efficiency, this model is conservative. To account fully for the observed throughput, we also had to make small upward adjustments in optical efficiency and detector quantum efficiency. Although this model nominally predicts an improvement in sensitivity, because of the 15% increase in assumed background it is in almost perfect agreement with the prelaunch value.

4.3 Model 2

Model 2 adjusts the read noise to a worst case value, to show that in 10 second DCEs the 24 μ m band is strongly background limited and that shortfalls in read noise will not significantly degrade the performance. Slightly larger impacts from degraded read noise would result in shorter integrations.

4.4 Model 3

Model 3 is a "best case" in which the photoconductive gain has been set to 0.85 and the instrument efficiencies adjusted to account for the observed signal. We retain the assumption of a 15% increase in sky brightness. The division of improved instrument efficiency between quantum efficiency and transmission is arbitrary.

4.5 Model 4

Model 4 is a "worst case" in which the photoconductive gain has been set to 1 and we have assumed a reduction in the calibration of electrons per DN. The instrument efficiencies have been adjusted to fit the observed signals. We have also assumed the worst case read noise.

4.6 Predicted Performance and Requirements

We conclude that the one-standard-deviation signal level under the conditions for Table 2 will be below 13 μ Jy, and is likely to be close to 11 μ Jy. The level 3 requirement on

sensitivity for this band was one sigma of $37\mu\text{Jy}$ on a point source at a background of $2.2 \times 10^{-17} \text{ W/pixel}$. If we input this background to the worst case model 4, and also increase the background by the indicated 15%, the predicted point source one sigma detection level is $15\mu\text{Jy}$. This band therefore exceeds the requirement by a factor of two.

Because the signals from stars are in units of DN, the saturation limits are independent of the various radiometric models and DN conversion factors. We have assumed that 96% of the dynamic range of the A/D converter can be used for the data (that is, that the detector output level is set to 4% above the low-signal rail). We then find that the saturation limits are:

- 7.8 Jy for first differences
- $\{[4.1 - 0.002 \times (\text{sky in MJy/sr})]\text{Jy}\}/(T_{\text{int}} - 0.5)$, where T_{int} is the nominal DCE time.

The nominal DCE operation includes a reset, and then a second half a second later, after which the integration ramp begins. Therefore, if an observer enters a DCE time of, say, 3 seconds, the instrument will provide an integration of 2.5 seconds, and the saturation limit will be that appropriate to 2.5 seconds. Therefore, the formula above should provide correct estimates independently of T_{int} . The instrument team had expressed a goal that the instrument should not saturate on a 0 magnitude star. This flux level translates to 7.5 Jy for this band, and this goal is met with essentially no margin. In normal observing, however, it is implausible that a star be centered systematically on a single pixel as has been assumed in the saturation calculation, so such a star will have significant margin against saturation in most images of a dithered sequence.

5. Recommended 24mm Parameters for Release

The SSC predicted sensitivity values for MIPS can now be revised and most of the margin removed. Table 3 gives numbers in terms of the one-standard-deviation flux limit on a point source per unit DCE. That is, to predict values achieved in an observation, these values should be divided by the square root of the number of DCEs on a source. The values are based on the "worst case" model, and therefore include the small margin implicit in that choice (about 15%).

Table 3. Predicted Sensitivity, one sigma per DCE, in mJy			
	16.1 MJy/sr	23.9 MJy/sr	65.6 MJy/sr
3 sec	473	538	801
4 sec	358	413	632
10 sec	183	218	357
30 sec	105	130	> 50% saturation level

Because the first difference is substituted for a saturated value, it can be advertised that the saturation limit for this band is 7.8Jy assuming a point source. Observers should be warned that values close to or above $\{[4.1 - 0.002 \times (\text{sky in MJy/sr})]\text{Jy}\}/(T_{\text{int}} - 0.5)$, where T_{int} is the nominal DCE time, will be based on this substitution.